Journal of Applied Electrochemistry (2005) 35:1191–1202
DOI 10.1007/s10800-005-9031-9

Modelling potentials, concentrations and current densities in porous electrodes for metal recovery from dilute aqueous effluents

C.Y. CHENG[1], G.H. KELSALL[1,*] and D. PILONE[1,2]
[1]*Department of Chemical Engineering, Imperial College London, London SW7 2AZ, UK*
[2]*Dip. ICMMPM, Università degli Studi di Roma "La Sapienza", Via Eudossiana, 18 00184 Roma, Italy*
*(*author for correspondence, e-mail: g.kelsall@imperial.ac.uk)*

Received 24 November 2004; accepted in revised form 14 April 2005

Key words: bipolar, felt electrodes, lead, lead dioxide, monopolar, Pb(II), porous electrodes

Abstract

One-dimensional steady-state models have been developed for the recovery of Pb(II) ions from lead–acid battery recycling plant effluent by simultaneous lead and lead dioxide deposition, including oxygen evolution/reduction and hydrogen evolution as loss reactions. Both monopolar and bipolar reactor with porous graphite electrodes were modelled, as a design aid for predicting spatial distributions of potentials, concentrations, current densities and efficiencies, as well as specific electrical energy consumptions and by-pass currents. Since the industrial effluent contains a large excess of supporting electrolyte (Na_2SO_4), the electrical migrational contribution to reactant transport rates was neglected and the current density–potential relationship was described by the Butler–Volmer equation, allowing for both kinetic and mass transport control. The models were implemented and the governing equations solved using commercial finite element software (FEMLAB). The effects were investigated of electrolyte velocity, applied cathode potential, dissolved oxygen concentration and inlet Pb(II) ion concentration on single-pass conversion, current efficiency and specific electrical energy consumptions. According to model predictions, de-oxygenation of the inlet process stream was found to be crucial to achieving acceptable (i.e. >0.8) current efficiencies. Bipolar porous electrodes were also determined to be inappropriate for the recovery of Pb(II) from effluents, as the low concentration involved resulted in the predicted fraction of current lost as by-pass current, i.e. current not flowing in and out of the bipolar electrode, to be greater than 90% for the ranges of the variables studied.

Notation

Symbol	Meaning (Units)
a	Specific surface area of porous electrode $m^2\ m^{-3}$
C_i	Concentration of species i mol m^{-3}
$C_{i,0}$	Inlet concentration of species i mol m^{-3}
D_i	Diffusion coefficient of species i $m^2\ s^{-1}$
d	Diameter of felt fibre m
d_h	Hydraulic diameter of felt fibre m
E_j	Equilibrium electrode potential vs. reference electrode V
E_j^0	Equilibrium electrode potential under standard conditions vs. reference electrode V
E_s	Specific electrical energy consumption kW h mol^{-1}
F	Faraday constant C mol^{-1}
i	Superficial current density A m^{-2}
I_l	Average liquid phase current over the whole electrode A
I_s	Average solid phase current over the whole electrode A
j	Current density of reactions A m^{-2}
j_0	Exchange current density of reaction A m^{-2}
j_L	Limiting current density of reaction A m^{-2}
k_m	Mass transport rate coefficient m s^{-1}
L	Length of the system being modelled m
La	Length of anode m
Lb	Length of bulk electrolyte m
Lc	Length of cathode m
n	Charge number of reaction
N_i	Flux of species i mol $m^{-2}\ s^{-1}$
U	Cell voltage V
V_c	Potential at feeder cathode electrode V
V_a	Potential at feeder anode electrode V
v	Linear electrolyte velocity m s^{-1}
v_{eff}	Solution velocity in the empty cross section area m s^{-1}
x	Horizontal distance from electrolyte inlet m
z_i	Number of charge on species i
α	Charge transfer coefficient
β	Tafel coefficient of reaction, i.e. $\alpha\ n\ F/(RT)$ V^{-1}
η_j	Overpotential of reaction j V

ϕ_s	Solid phase potential V
ϕ_l	Liquid phase potential V
$\phi_{l,cell}$	Liquid phase potential difference applied across the bipolar electrode V
σ_s	Solid phase conductivity s m^{-1}
σ_l	Liquid phase conductivity s m^{-1}
$\sigma_{l,0}$	Pure liquid phase (electrolyte) conductivity s m^{-1}
$\upsilon_{i,j}$	Stoichiometric coefficient of species i in reaction j
υ	Kinematic viscosity m^2 s^{-1}
ε	Voidage of the graphite felt electrode
Φ_j	Current efficiency of reaction j
$\Phi_{j,mean}$	Average current efficiency of reaction j
$\Phi_{bp,mean}$	Average fraction of total current lost as by-pass current
i	Subscript i refers to reacting species
j	Subscript j refers to reactions

1. Introduction

Electrolytic reactors can be used to solve environmental problems, as they can form the basis of clean and elegant processes for treating effluents and wastes. Many industrial processes produce low concentrations of heavy metals in aqueous effluents, which have to be depleted to concentrations typically $\leq$1 ppm before they can be discharged to sewers. Conventional processes use lime to precipitate metal compounds, but disposal of such solids in landfill sites, other than in those specially licensed, will be precluded in the future. By contrast, electrolytic reactors can achieve such target concentrations, by electrodeposition of the contained metals, which can then be recycled. However, low dissolved metal concentrations imply low rates of electrodeposition and competing loss reactions, so reactors need to be designed for optimal efficiency, using figures of merit such as kW h per tonne of metal recovered. Reactors with porous electrodes are the preferred option, as their high surface area allows low current densities at the electrode/electrolyte interface, while maintaining high reaction rates per unit volume of reactor, relative to reactors with planar electrodes or low porosity electrodes. Therefore, mathematical models for porous electrodes are required to predict the behaviour of different types of electrochemical reactors, to aid reactor design and performance optimisation.

Newman [1] developed one-dimensional equations to describe the macroscopic behaviour of a single reaction in a flow-through porous electrode. Many models were developed subsequently, based on Newman's equations. Trainham [2] applied them to a metal recovery system, allowing for simultaneous hydrogen evolution as a side reaction. Doherty [3] obtained analytical solutions for porous electrodes operating under transport limited current conditions and numerical solutions for the electron transfer controlled regime. Saleh's model [4] accounted for gas evolution and investigated the effect of bubble formation in changing the effective electrolyte conductivity. Bisang [5] discussed the effects of different parameters on optimisation of the performance of porous electrodes, assuming kinetically-controlled reaction rates. Modelling of one-dimensional flow-through porous electrodes is a well-developed subject, of which there are detailed accounts in several monographs [6–8]. However, a definitive description of the porous electrode behaviour requires a synthesis of the various models that have been published hitherto.

Rousar [9], Bisang [10] and Scott [11] developed models for flow-by bipolar reactors with planar electrodes and Goodridge and King developed equations to estimate the minimum energy consumption for bipolar packed-bed electrodes [12] and fluidised bipolar bed electrodes [13]. The only report found of a (one-dimensional) model of a reactor with a porous bipolar electrode [14], involved its operating under fully flooded conditions, with a single reversible reaction.

The objective of the work described below was to develop steady-state models to predict the behaviour of monopolar and bipolar reactors with porous electrodes for removal of Pb(II) ions from dilute liquid effluents, arising e.g. from battery or battery recycling plants. The feasibility of simultaneous cathodic deposition of lead and anodic deposition of lead dioxide from dilute aqueous effluents containing low concentrations of Pb(II) ions, has been established experimentally [15, 16], enabling Pb(II) concentrations to be depleted to <60 ppb in a batch recycle reactor with graphite felt electrodes [16].

2. Reaction system

2.1. *Electrochemical reactions*

The aqueous effluent from the lead–acid battery recycling plant has a slightly alkaline pH, so Pb(II) is present in the form of $HPbO_2^-$ ions. The Pb(II) ions are removed simultaneously by cathodic deposition of lead:

$$HPbO_2^- + H_2O + 2e^- \rightarrow Pb + 3OH^- \quad (1)$$

and anodic deposition of lead dioxide:

$$HPbO_2^- + OH^- \rightarrow PbO_2 + H_2O + 2e^- \quad (2)$$

The loss reactions are primarily reduction of oxygen and hydrogen evolution at the cathode:

$$O_2 + 2H_2O + 4e^- \rightarrow 4OH^- \quad (3)$$

$$2H_2O + 2e^- \rightarrow H_2 + 2OH^- \quad (4)$$

and oxygen evolution at the anode:

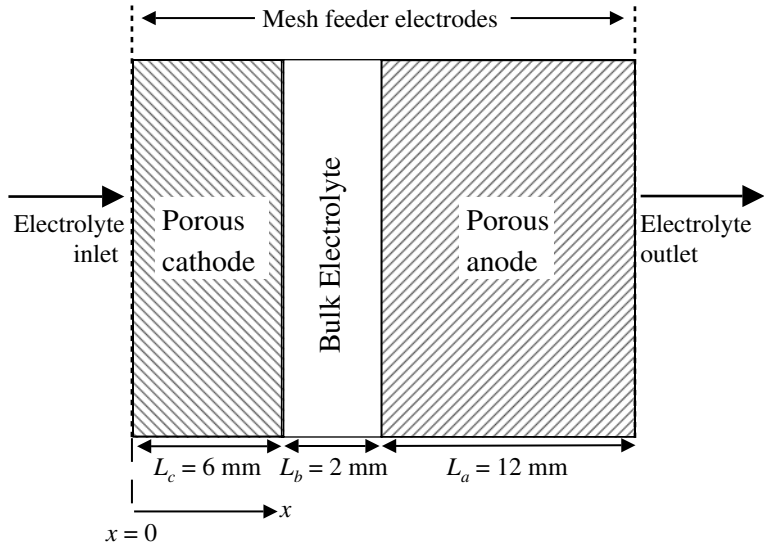

Fig. 1. Schematic representation of a flow-through monopolar reactor.

$$4OH^- \rightarrow O_2 + 2H_2O + 4e^- \quad (5)$$

A pH of 13 was used in experimental work, to ensure adequate Pb(II) solubility; the calculated minimum cell voltage for simultaneous deposition of lead (1) and lead dioxide (2) at that pH is ca. 0.9 V.

2.2. *Electrochemical reactors*

Mathematical models for two types of reactor were developed: a flow-through reactor with monopolar electrode arrangement, shown schematically in Figure 1, and a single flow-through bipolar electrode, shown in Figure 2. The porous electrodes in the reactors are all graphite felt electrodes with an assumed effective specific surface area of 5000 $m^2\ m^{-3}$.

3. Mathematical models

The following assumptions were made to simplify the equations, which, in the first instance, refer to a one-dimensional model, as implied by the flow-through reactors shown schematically in Figures 1 and 2:

(a) The system operates at steady state without structural change or insulation effects, i.e. the properties of the electrodes remain constant with time.
(b) Electrodes' porosities and conductivities of both solid and liquid phases are uniform within the spatial domain concerned and hence, ohm's law is applicable to both phases.
(c) Excess non-reactive supporting electrolyte is present, so electrical migrational transport of the reactive species is insignificant.
(d) Electrolyte is under forced plug flow in the direction of current flow, with a uniform velocity distribution.
(e) The kinetics of deposition of Pb by reaction (1) and PbO_2 by reaction (2) and oxygen reduction by reaction (3), may be described by the Butler–Volmer equation, Equations (6), (7) and (8), respec-

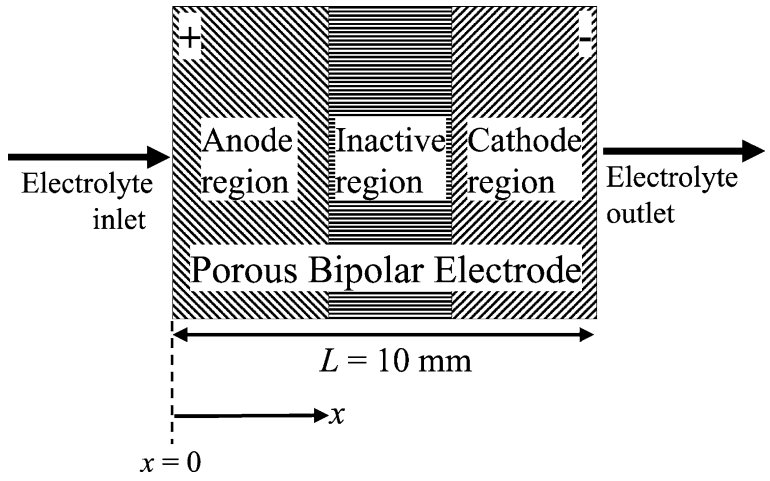

Fig. 2. Schematic representation of a single flow-through bipolar electrode.

tively, allowing for both kinetic and mass transport control:

$$j = \frac{j_{0,\mathrm{Pb}}\left[\exp\left\{\frac{(1-\alpha_j)n_jF}{\mathrm{RT}}\eta\right\} - \exp\left\{-\frac{\alpha_j n_j F}{\mathrm{RT}}\eta\right\}\right]}{1 + \left(\frac{j_{0,\mathrm{Pb}}}{j_{L,\mathrm{Pb}}}\right)\exp\left\{-\frac{\alpha_j n_j F}{\mathrm{RT}}\eta\right\}} \quad (6)$$

$$j = \frac{j_{0,\mathrm{PbO_2}}\left[\exp\left\{\frac{(1-\alpha_j)n_jF}{\mathrm{RT}}\eta\right\} - \exp\left\{-\frac{\alpha_j n_j F}{\mathrm{RT}}\eta\right\}\right]}{1 + \left(\frac{j_{0,\mathrm{PbO_2}}}{j_{L,\mathrm{PbO_2}}}\right)\exp\left\{\frac{(1-\alpha_j)n_jF}{\mathrm{RT}}\eta\right\}} \quad (7)$$

$$j = \frac{j_{0,\mathrm{O_2}}\left[\exp\left\{\frac{(1-\alpha_j)n_jF}{\mathrm{RT}}\eta\right\} - \exp\left\{-\frac{\alpha_j n_j F}{\mathrm{RT}}\eta\right\}\right]}{1 + \left(\frac{j_{0,\mathrm{O_2}}}{j_{L,\mathrm{O_2}}}\right)\exp\left\{-\frac{\alpha_j n_j F}{\mathrm{RT}}\eta\right\}} \quad (8)$$

(f) Hydrogen evolution by reaction (4) and oxygen evolution by reaction (5) are both under kinetic control and their current density is estimated by one of the limiting forms of the Butler–Volmer equation, Equations (9) and (10), respectively.

$$j = -j_{0,\mathrm{H_2}}\exp\left\{-\frac{\alpha n_i F}{\mathrm{RT}}\eta\right\} \quad (9)$$

$$j = j_{0,\mathrm{O_2}}\exp\left\{\frac{(1-\alpha)n_iF}{\mathrm{RT}}\eta\right\} \quad (10)$$

(g) The solid and liquid phases have position-independent conductivities and obey ohm's law:

$$i = -\sigma\frac{\partial\phi}{\partial x} \quad (11)$$

where i is the superficial current density.

3.1. *Kinetic parameters*

The exchange current densities (j_0) and Tafel coefficients for the deposition of elemental lead and lead dioxide [17], the reduction and evolution of oxygen [17] and evolution of hydrogen [18], are derived based on experimental data obtained from the literature.

$$j_{0,\mathrm{Pb}} = 280.59 \times \left(C_{\mathrm{Pb^{(II)}}}\right)^{0.20}\mathrm{A\,m^{-2}};$$

$$\beta_{\mathrm{Pb}} = -31.15\,\mathrm{V^{-1}} \quad (12)$$

$$j_{0,\mathrm{PbO_2}} = 0.42 \times \left(C_{\mathrm{Pb^{(II)}}}\right)^{0.76}\mathrm{A\,m^{-2}};$$

$$\beta_{\mathrm{PbO_2}} = 9.35\,\mathrm{V^{-1}} \quad (13)$$

$$j_{0,\mathrm{O_2}} = 10^{-6}\,\mathrm{A\,m^{-2}}; \quad \beta_{\mathrm{O_2}} = 19.46\,\mathrm{V^{-1}} \quad (14)$$

$$j_{0,\mathrm{H_2}} = 0.0034\,\mathrm{A\,m^{-2}}; \quad \beta_{\mathrm{H_2}} = -17.85\,\mathrm{V^{-1}} \quad (15)$$

The overpotential, η_j, is calculated by:

$$\eta_j = \phi_s - \phi_l - E_j \quad (16)$$

where the equilibrium potential of reaction j, was calculated from the Nernst equation:

$$E_j = E_j^0 + \frac{\mathrm{RT}}{nF}\ln\left(\frac{\prod C_{i,\mathrm{O}}^{\upsilon_{i,j}}}{\prod C_{i,R}^{\upsilon_{i,j}}}\right) \quad (17)$$

3.2. *Behaviour of Felt electrodes*

The following correlation [19] was used to estimate mass transport coefficients:

$$k_m = 3.19\left(\frac{D_i}{d_h}\right)\left(\frac{vd_h}{\upsilon}\right)^{0.69} \quad (18)$$

$$d_h = \frac{4\varepsilon}{(4/d)(1-\varepsilon)} \quad (19)$$

as it appeared to be the most appropriate of those reported, having been determined for carbon felt used for electrodeposition of heavy metals.

The effective liquid phase conductivity in the felts was estimated by the Bruggeman [20] equation:

$$\sigma_\mathrm{l} = \sigma_{\mathrm{l},0}\,{}^{*}\varepsilon^{1.5} \quad (20)$$

where ε is the fraction of volume occupied by the liquid phase in the porous electrode.

The conductivity of the solid phase was estimated by a correlation specifically for graphite-felt electrodes [21]:

$$\sigma_\mathrm{s} = 10 + 2800^{*}\left(1 - \frac{\varepsilon}{\varepsilon_0}\right)^{1.55} \quad (21)$$

where ε_0 is the voidage before mechanical compression of the felt.

Due to high contact resistance between graphite fibres, graphite felt electrodes should not be treated as continuous solid matrices. The conductivity of graphite felt is of the same order as the ionic conductivity of strong aqueous electrolytes. In this model, it is assumed that the graphite felt electrode is not subjected to mechanical compression, i.e. $\varepsilon = \varepsilon_0$. The effects of changing the electrode phase conductivity by electrodeposition of Pb or PbO_2 were shown to have negligible effect on the potential and current distributions at the low current densities corresponding to the low concentrations of Pb(II) reactant envisaged. However, that would not be the case for higher concentrations, at which far higher conductivities would be achieved than predicted by Equation (21) for the graphite felt alone.

Within the porous electrode, any change of current density (i_l) in the liquid phase results from current density (j) crossing the electrode/electrolyte interface by reaction:

$$\frac{di_\mathrm{l}}{dx} = aj \quad (22)$$

A current balance requires:

$$\frac{di_s}{dx} + \frac{di_l}{dx} = 0 \tag{23}$$

Differentiating Equation (11) and substituting from Equations (22) and (23), results in the partial differential equations relating the potential distribution in the solid and liquid phases of the porous electrode, and the reaction current density:

$$\frac{d^2\phi_s}{dx^2} = -\frac{aj}{\sigma_s} \tag{24}$$

$$\frac{d^2\phi_l}{dx^2} = \frac{aj}{\sigma_l} \tag{25}$$

In the bulk electrolyte between the two electrodes in the monopolar reactor, no homogeneous reaction occurs and the concentration is assumed to be constant, so the potential varies according to ohm's law, Equation (11).

In the presence of excess supporting electrolyte, the contribution of electrical migration of reacting species is negligible to the overall rate of mass transfer, which is dominated by diffusion and convection. Plug flow of electrolyte was assumed with uniform velocity across the reactor. A material balance in the liquid phase within the porous electrode is represented by:

$$D_i\varepsilon\frac{d^2C_i}{dx^2} - v\frac{dC_i}{dx} = \sum_j \frac{\upsilon_{i,j}aj_j}{n_jF} \tag{26}$$

As no reaction occurs within the bulk electrolyte, the concentration is constant, so:

$$\frac{dC_i}{dx} = 0 \tag{27}$$

3.3. *Monopolar electrode*

The model for the monopolar reactor is divided into three sub-domains: cathode, bulk electrolyte and anode. The boundary conditions for the four boundaries are specified below.

At the cathode feeder electrode, at $x = 0$:

$$\phi_s = V_c; \quad \frac{d\phi_l}{dx} = 0; \quad C_i = C_{i,0} \tag{28}$$

where V_c is the applied cathode potential, and $C_{i,0}$ is the inlet concentration of component i.

At the interface between the porous cathode and bulk electrolyte, at $x = \mathrm{Lc}$:

$$\frac{d\phi_s}{dx} = 0; \quad \phi_l = 0; \quad C_i = C_{i,(x=\mathrm{Lc})} \tag{29}$$

At the interface between the bulk electrolyte and the porous anode, at $x = \mathrm{Lc} + \mathrm{Lb}$:

$$\frac{d\phi_s}{dx} = 0; \quad \phi_l = \phi_{l(x=\mathrm{Lc}+\mathrm{Lb})}; \quad C_i = C_{i,(x=\mathrm{Lc}+\mathrm{Lb})} \tag{30}$$

At the anode feeder electrode, at $x = \mathrm{Lc} + \mathrm{Lb} + \mathrm{La}$

$$\phi_s = V_a; \quad \frac{d\phi_l}{dx} = 0; \quad N_i = vC_i \tag{31}$$

The potential of the anode feeder electrode, V_a, was chosen by trial and error, such that anodic and cathodic current were equal and opposite. Where current is carried in one phase only, the potential gradients will then be $\partial\phi_s/\partial x = -i/\sigma_s$ at the boundaries between feeder electrodes and felt, and $\partial\phi_l/\partial x = -i/\sigma_l$ between felt and bulk electrolyte. It was also assumed that convective flux is dominant at the exit of the reactor, i.e. at the anode feeder electrode, as was the case throughout the reactor.

3.4. *Bipolar reactor*

The boundary conditions for the two boundaries to the single domain in the model for the bipolar electrode are specified below.

At the inlet of the bipolar electrode, $x = 0$:

$$\phi_s = \phi_{s,\mathrm{in}}; \quad \phi_l = \phi_{l,\mathrm{cell}}; \quad C_i = C_{i,0} \tag{32}$$

At the outlet of the bipolar electrode, $x = L$:

$$\frac{d\phi_s}{dx} = 0; \quad \phi_l = 0; \quad \frac{dC_i}{dx} = 0 \tag{33}$$

$\phi_{s,\mathrm{in}}$ is the solid phase potential at the inlet of the bipolar electrode, its value chosen so that anodic and cathodic currents were equal and opposite. $\phi_{l,\mathrm{cell}}$ is the cell voltage in the liquid phase across the bipolar electrode, which is a controlled variable in the bipolar reactor model.

4. Results and discussion

4.1. *Monopolar reactor – potentials, concentrations and current densities*

Figure 3 shows the potential profiles in liquid and solid phases at an applied cathode potential of −0.7 V (SHE). At the feeder electrodes, the potential gradient in the liquid phase is zero as all the current is in the solid phase. The liquid phase potential gradients increase towards the bulk electrolyte as current is being transferred from the solid to liquid phase. The opposite occurs for solid phase potential, with the largest potential gradient at the feeder electrodes ($\partial\phi_s/\partial x = i/\sigma_s$) and zero gradients at the electrode and bulk electrolyte interfaces. The liquid and solid phase potential profiles are mirror images of each other as all current leaving the solid phase must enter the liquid phase. For the low reactant concentrations and hence low current densities used, the potential drop within the bulk electrolyte between anode and cathode was only about 0.5 mV.

Figure 4 shows the concentration profiles of Pb(II) ions within the three regions in a monopolar reactor. Pb(II) ions are removed in the cathode and anode by

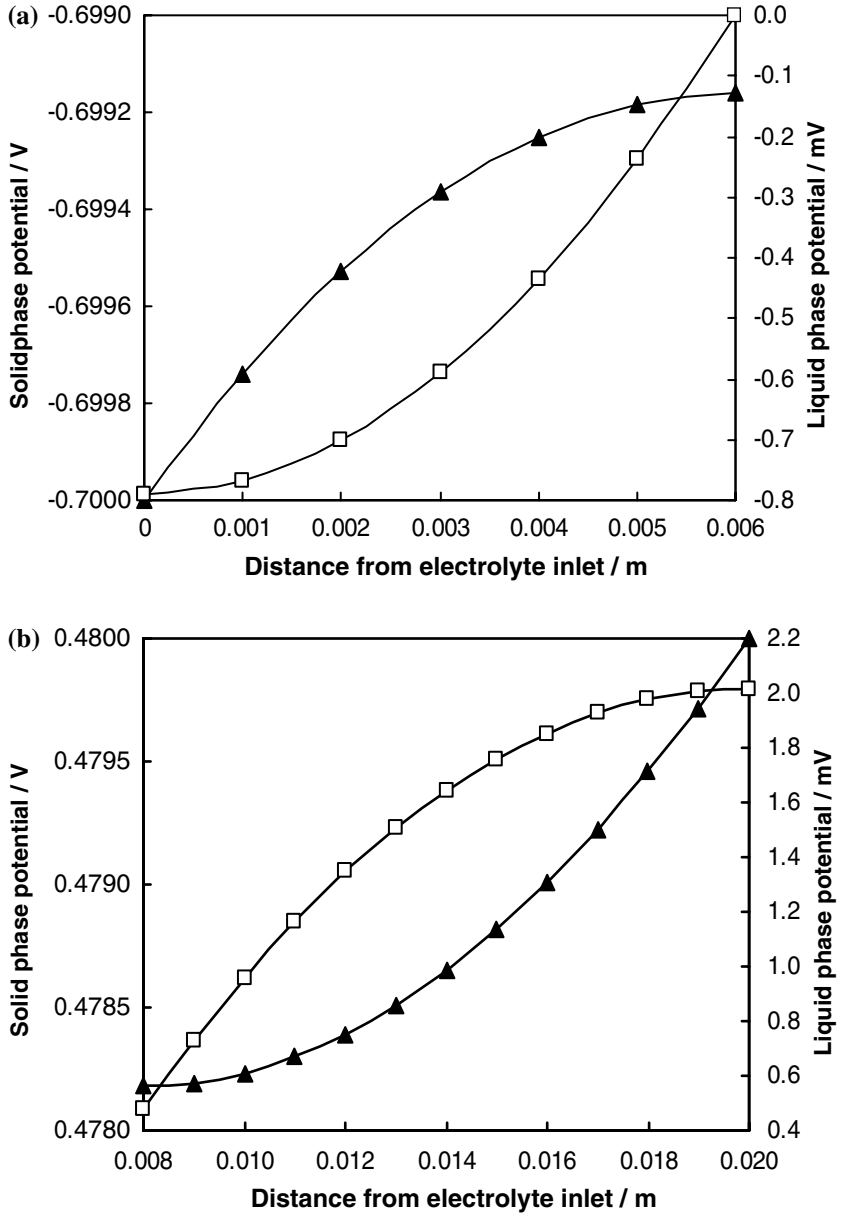

Fig. 3. Potential profiles of solid (▲) and liquid (□) phases in cathode (a) and anode (b), for the monopolar reactor with an applied cathode potential of −0.7 V (SHE).

lead and lead dioxide deposition by reactions (1) and (2), respectively. In the bulk electrolyte between anode and cathode, since there is no homogeneous reaction, Pb(II) concentration remains constant. As the applied cathode potential was decreased, Pb(II) ions were depleted to a greater extent, until at ca. −0.9 V (SHE), mass transport control was achieved. However, although the concentration profiles for −0.9 V and −1 V (SHE) are similar, lower potentials resulted in greater loss of current to side reactions with consequential decreasing current efficiencies.

At pH 13, the hydrogen and oxygen evolution side reactions are both preventable in principle, by judicious control of cathode and anode potential, respectively. At the cathode, as the reversible potential of hydrogen evolution (≈ −0.8 V (SHE)) is more negative than that of lead deposition (≈ −0.6 V (SHE)), in the window between the two potentials, lead deposition will occur in the absence of hydrogen evolution. Similarly at the anode, the reversible potential of oxygen evolution (≈0.45 V (SHE)) is more positive than that of lead dioxide deposition (≈0.35 V (SHE)), so lead dioxide deposition could occur in the absence of oxygen evolution. This is shown by the effect of applied cathode potentials on cathode current densities in Figure 5a and the effect of corresponding anode potentials on anode current densities Figure 5b. At large applied cathode potentials, e.g. < −0.9 V (SHE), hydrogen evolution at the cathode and oxygen evolution at the anode are at comparative rates to the main

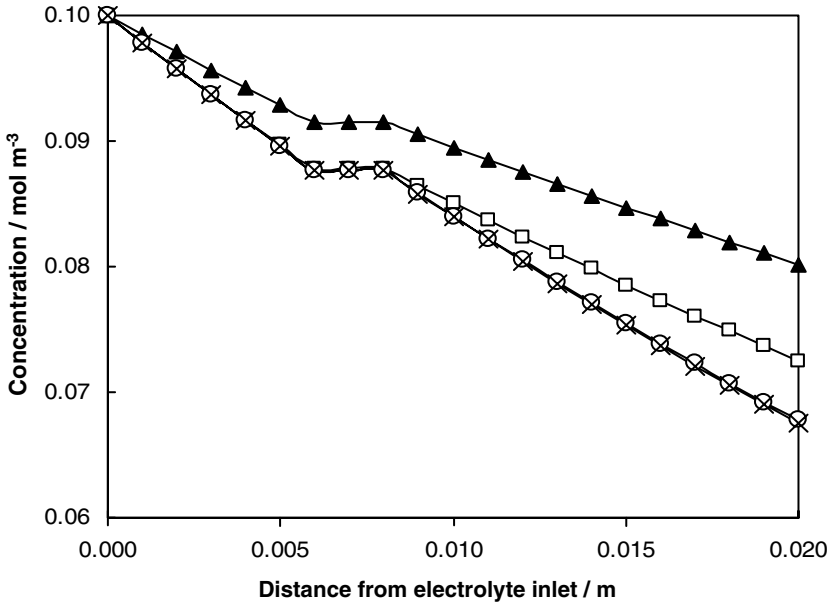

Fig. 4. Effect of cathode potential on Pb(II) concentration profiles in the monopolar reactor, with an electrolyte velocity of 0.001 m s^{-1}, an inlet Pb(II) concentration of 0.1 mol m^{-3} and an inlet dissolved oxygen concentration of 0.01 mol m^{-3}. Applied cathode potential, V_c, equals −0.6 V (SHE) (▲) , −0.7 V (SHE) (□) , −0.9 V (SHE) (○) and −1 V (SHE) (×).

reactions. Reduction of oxygen is unavoidable and it is predicted to be mass transport controlled at potentials <0.35 V (SHE) [16].

4.2. *Performance comparison*

The current efficiency, single-pass conversion of Pb(II) ions and the specific electrical energy consumption were used to compare the performance of electrochemical reactors. Cathodic and anodic current efficiencies for Pb(II) ion recovery were calculated from:

$$\Phi_{Pb} = \frac{j_{Pb}}{j_{Pb} + j_{O_2(Red)} + j_{H_2}} \tag{34}$$

$$\Phi_{PbO_2} = \frac{j_{PbO_2}}{j_{PbO_2} + j_{O_2(Ox)}} \tag{35}$$

Oxygen reduction is an unpreventable side reaction that is mass transport controlled. Figure 6 shows the average current efficiency as a function of inlet dissolved oxygen concentrations, ranging from 10^{-5} to 1.28 mol m^{-3}, the maximum dissolved oxygen concentration under atmospheric pressure estimated using a correlation developed by Tromans [22]. In the worst-case, i.e. inlet oxygen concentration at 1.28 mol m^{-3}, the average current efficiency was predicted to be <0.05, so that deoxygenating the inlet stream is essential to obtain acceptable current efficiencies. Current efficiencies of >0.9 can be achieved with an inlet oxygen concentration of 0.01 mol m^{-3}, which was used in all the subsequent simulations.

Figure 7 shows that current efficiencies were predicted to decrease with decreasing cathode potential, as expected. Single-pass conversion of Pb(II) increased with decreasing cathode potential in the range −0.6 V (SHE) to −0.9 V (SHE). For cathode potentials <−0.9 V (SHE), mass transport limited current densities for electrodeposition of lead and lead dioxide was approached, so cathode potential had little effect on current density and conversion. With an inlet Pb(II) concentration of 0.01 mol m^{-3} and an electrolyte velocity of 0.001 m s^{-1}, the maximum single-pass conversion attained was limited to 0.3 and current efficiencies decreased with decreasing cathode potential.

Increases in electrolyte velocity enhance mass transport rates but decrease residence times of reacting species, so decreasing single-pass conversion of Pb(II). As electrolyte velocity was increased from 10^{-5} to 10^{-4} m s^{-1}, average current efficiencies increased from 0.6 to 0.9. Further increase in electrolyte velocity shows no significant effect on current efficiency. As electrolyte velocity increased from 10^{-5} to 10^{-1} m s^{-1}, the single-pass conversion of Pb(II) decreased from 0.8 to 0.1, as shown in Figure 8. Therefore, an optimal electrolyte flow rate exists to achieve a balance between current efficiency and single-pass conversion, but pumping costs also need to be considered. At low single-pass conversions, a recycle stream would be required to achieve the consent Pb(II) concentration of <1 ppm (ca. 5×10^{-3} mol m^{-3}). Therefore, partial recycle operation would be expensive for high effluent flow rates and hence, single-pass operation is preferred.

The specific electrical energy consumption, Es (kW h (mol of Pb(II) removed)$^{-1}$), can be used as a figure of merit used to compare the performance of different reactor configurations and operating conditions:

$$E_s = \frac{2FU}{3.6 \times 10^6(\Phi_{Pb,mean} + \Phi_{PbO_2,mean})} \tag{36}$$

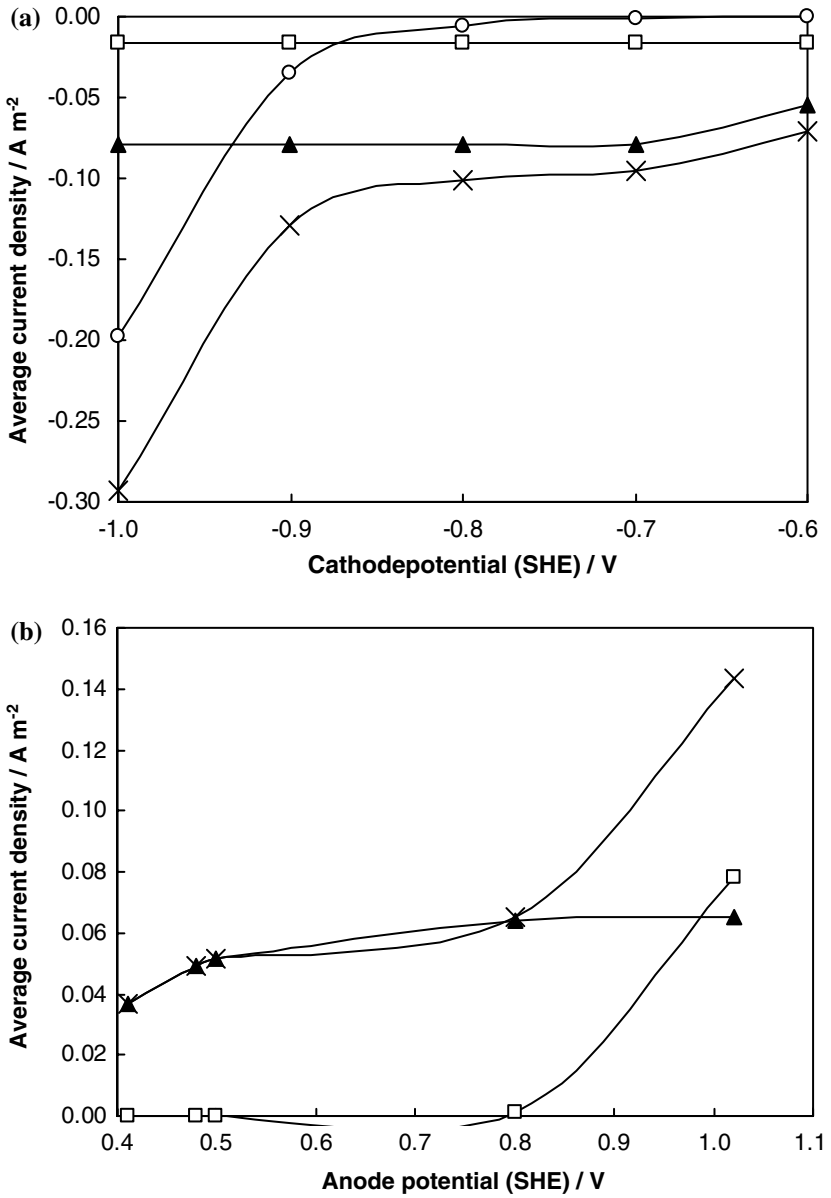

Fig. 5. (a) Effect of cathode potential on average current densities (j) in the monopolar reactor cathode, with inlet Pb(II) concentration of 0.1 mol m^{-3}, inlet dissolved O_2 concentration of 0.01 mol m^{-3} and electrolyte velocity of 0.001 m s^{-1}. Current densities of reduction of oxygen (□) , hydrogen evolution (○), lead deposition (▲) and total cathode current density (×) at applied cathode potential between −0.6 V (SHE) and −1 V (SHE). (b) Effect of anode potential on average current densities (j) in the monopolar reactor anode, with inlet Pb(II) concentration of 0.1 mol m^{-3}, inlet dissolved O_2 concentration of 0.01 mol m^{-3} and electrolyte velocity of 0.001 m s^{-1}. Current densities of oxygen evolution (□) , lead dioxide deposition (▲) and total anode current density (×) at anode potentials ranged between 0.41 V (SHE) and 1.02 V (SHE).

Figure 9 shows that for an inlet Pb(II) concentration of 0.1 mol m^{-3}, the lowest specific electrical energy consumption occurs at an electrolyte velocity of 10^{-4} m s^{-1} and an applied cathode potential of −0.6 V (SHE).

However, as the single-pass conversion of Pb(II) under these operating conditions is only 0.4, recycling for the process stream would be necessary in order to achieve Pb(II) consent concentrations; this would increase the pumping energy requirement and hence overall operating costs. Longer path lengths, and hence higher conversions, are achievable with flow-by reactors, in which electrolyte flows normal to the current, rather than in parallel, as in the flow-through reactor described here. The behaviour of a flow-by reactor will be reported in a future publication, including a 2D model, which will also enable minimisation of (capital + running) costs, incorporating de-oxygenation costs, and so provide a rational basis for refining reactor design and operating conditions.

4.3. *Bipolar reactor*

Capital costs of bipolar reactors are generally lower than for equivalent monopolar reactors, but the latter's operating costs are predicted to be lower.

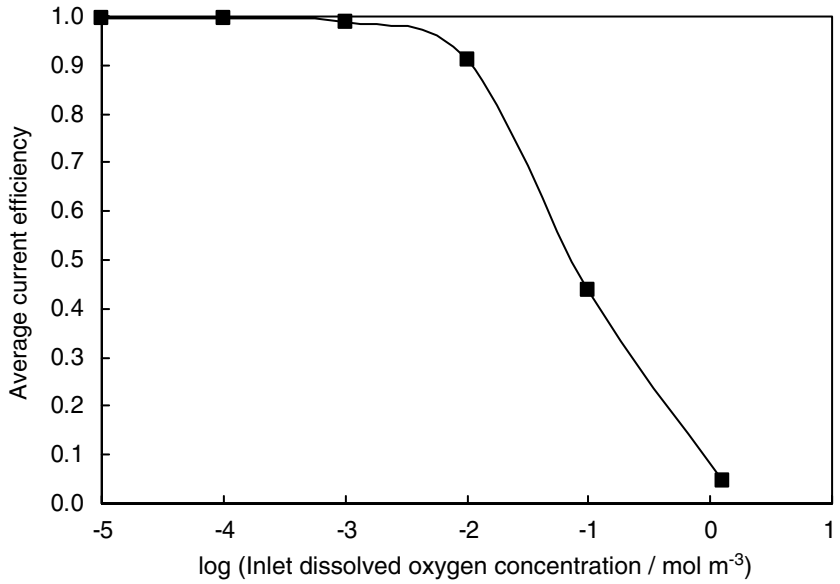

Fig. 6. Effect of inlet dissolved oxygen concentration on current efficiencies with Pb(II) concentration of 0.1 mol m^{-3}, an applied cathode potential of −0.65 V (SHE) and an electrolyte velocity of 0.001 m s^{-1}.

The major problem of a bipolar reactor is the loss of efficiency through by-pass current, i.e. current that continues to flow in the electrolyte (l) within the porous electrode, rather than flowing in and out of the solid phase (s) of the porous bipolar electrode. The fraction of total current ($I_l + I_s$) lost as by-pass current averaged over the entire porous electrode, $\Phi_{bp,mean}$, is defined by:

$$\Phi_{bp,mean} = \frac{I_l}{I_l + I_s} \tag{37}$$

where

$$I_s = -\sigma_s \frac{\partial \phi_s}{\partial x} \tag{38}$$

and

$$I_l = -\sigma_l \frac{\partial \phi_l}{\partial x} \tag{39}$$

The by-pass current depends on liquid and solid phase conductivities, exchange current densities, limiting current densities and the reactor configuration.

Both fully flooded porous electrodes and thin falling film operation were considered. In the fully flooded case, the pores of the porous electrode are completely filled with electrolyte and the liquid volume fraction equals the electrode porosity, i.e. 0.95 in this case. In the falling film operation, solid, liquid and gas phase co-exist in the

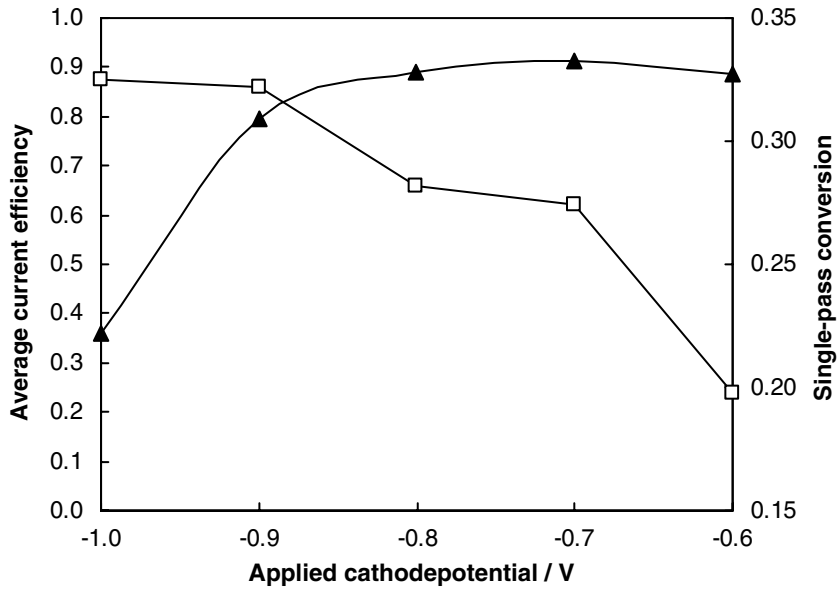

Fig. 7. Effect of cathode potential on average current efficiencies (▲) and single-pass conversions (□) at an inlet Pb(II) concentration of 0.1 mol m^{-3} and an electrolyte velocity of 0.001 m s^{-1}.

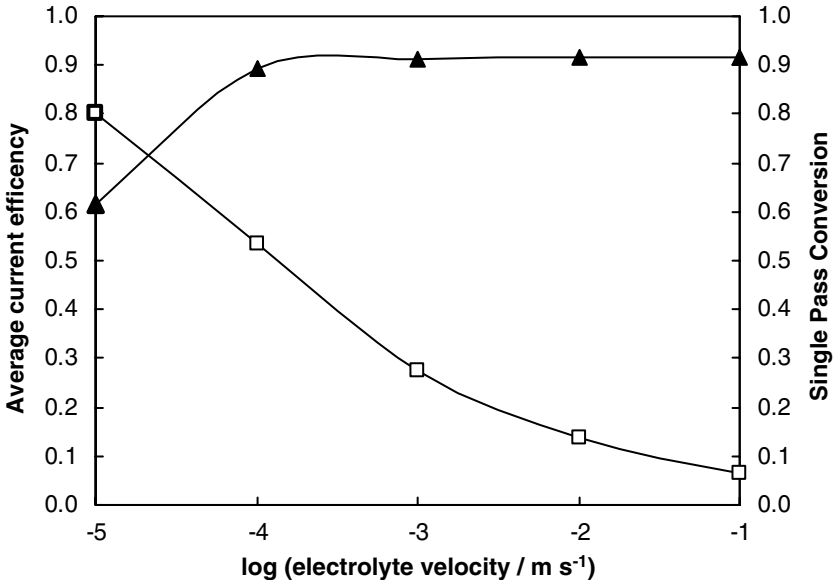

Fig. 8. Effect of electrolyte velocity on average current efficiency (▲) and single-pass conversion (□) with an inlet Pb(II) concentration of 0.1 mol m^{-3} and an applied cathode potential of −0.7 V (SHE).

porous electrode. The volume fraction occupied by the liquid phase varies with the thickness of the liquid film, which in turn affects the liquid phase conductivity, effective electrolyte velocity and mass transfer coefficient. As liquid volume fraction decreases, the liquid phase conductivity decreases, so decreasing the by-pass current.

According to Figure 10, with an inlet Pb(II) concentration of 0.1 mol m^{-3}, the by-pass current fraction is 0.9, even with a liquid volume fraction as low as 0.05. Therefore, it can be concluded that bipolar electrodes, under either fully flooded or falling film operation, are predicted to be inefficient to remove Pb(II) ions from lead-acid battery effluent by simultaneous lead and lead dioxide deposition. This is due to the low mass transfer limiting current density caused by the low Pb(II) concentration. However, at higher inlet concentrations, i.e. greater than 100 mol m^{-3}, current densities may not be limited by mass transfer rates and by-pass current fractions lower than 0.1 can be achieved with a cell voltage of 1.5 V.

5. Conclusions

(a) One dimensional models for Pb(II) ions recovery from lead–acid battery effluent by simultaneous lead and lead dioxide deposition have been

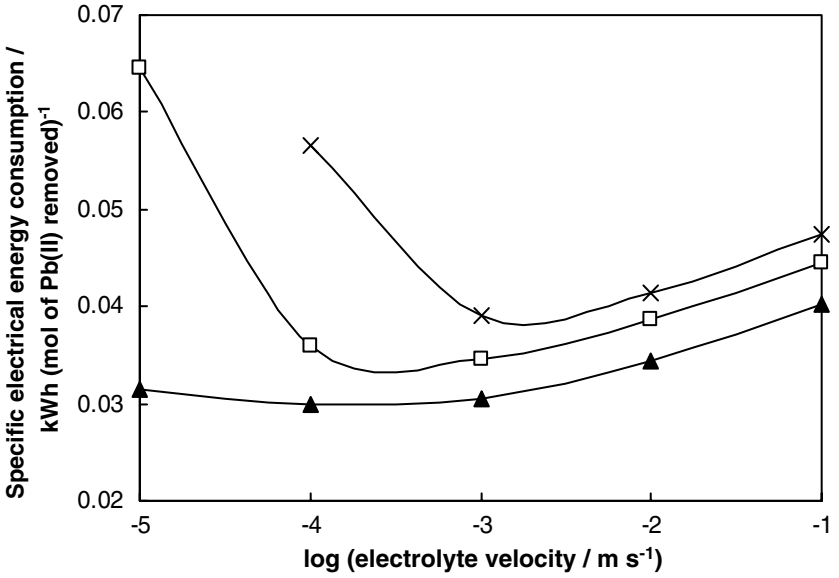

Fig. 9. Effect of the electrolyte velocity on specific electrical energy consumption, with an inlet Pb(II) concentration of 0.1 mol m^{-3}, at applied cathode potentials at −0.6 V (SHE) (▲) , −0.7 V (SHE) (□) and −0.8 V (SHE) (×).

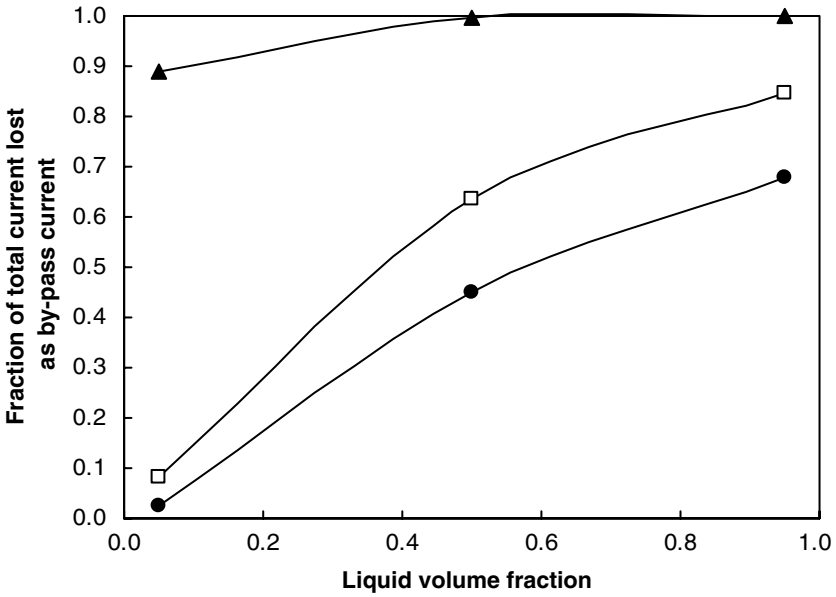

Fig. 10. Effect of liquid volume fraction on the fraction of total current lost as by-pass current, for inlet Pb(II) concentrations of 0.1 (▲), 100 (□) and 10000 (●) mol m^{-3}, at a cell voltage of 1.5 V and an electrolyte velocity of 0.001 m s^{-1}.

developed and implemented in FEMLAB for two systems: a monopolar reactor with porous electrodes and a single bipolar porous electrode, both with flow-through electrolyte arrangements and considering oxygen evolution/reduction and hydrogen evolution as loss reactions.

(b) According to model predictions for the monopolar reactor, electrolyte velocity has the greatest influence on single-pass conversion of Pb(II) ions. Deoxygenating the inlet stream to oxygen concentrations ≤ 0.01 mol m^{-3} enabled current efficiencies >0.9 to be achieved. With such electrolytes, cathode feeder electrode potentials of −0.6 to −0.7 V (SHE) resulted in current efficiencies of ca. 0.9 and specific electrical energy consumptions of <0.1 kW h (mol Pb(II) removed)$^{-1}$, for electrolyte velocities $>10^{-4}$ m s^{-1}. For the particular monopolar reactor design, conversions per pass decreased from 0.8 at 10^{-5} m s^{-1} to 0.1 at 10^{-1} m s^{-1}.

(c) Removal of lead (II) ions by the monopolar system demonstrated better performance than the bipolar system. According to model predictions, a single-pass conversion of 0.5 and a specific electrical energy consumption of less than 0.1 kW h per mole of Pb(II) ions removed is achievable with a monopolar reactor, operating at a cell voltage of −1.2 V and an electrolyte velocity of 10^{-4} m s^{-1}. In the bipolar case, only 35% of the porous electrode was predicted to be utilised. More importantly, due to the low Pb(II) concentrations and significant thermodynamic requirement of the reactions, more than 0.99 of the total current was predicted to be lost as by-pass current in a single bipolar porous electrode, operating under fully flooded condition. Even with falling film operation, with a liquid volume fraction of as little as 0.05, the by-pass current decreased only to 0.9.

References

1. J.S. Newman and C.W. Tobias, *J. Electrochem. Soc.* **109** (1962) 1183.
2. J.A. Trainham and J. Newman, *J. Electrochem. Soc.* **124** (1977) 1528.
3. T. Doherty, J.G Sunderland, E.P.L. Roberts and D.J Pickett, *Electrochim. Acta* **41** (1996) 519.
4. M.M. Saleh, *Electrochim. Acta* **45** (1999) 959.
5. J.M. Bisang, K. Juttner and G. Kreysa, *Electrochim. Acta* **39** (1994) 1297.
6. I. Rousar, K. Micka and A. Kimla, *Electrochemical Engineering II* (Parts D–F). (Elsevier, Amsterdam, 1986) pp. 109.
7. J.S. Newman, *Electrochemical Systems* (Prentice-Hall, Englewood Cliffs, NJ, 1991), Ch 22, p. 454.
8. Yu.A. Chizmadzhev and Yu.G. Chirkov, *in* E. Yeager, J.O.M. Bockris, B.E. Conway and S. Sarangapani (Eds), 'Comprehensive Treatise of Electrochemistry' vol. 6 (Plenum Press, New York, 1983), p. 317.
9. I. Rousar, *J. Electrochem. Soc.* **116** (1969) 676.
10. J.M. Bisang, *J. Appl. Electrochem.* **23** (1993) 966.
11. K. Scott, *Electrochim. Acta* **28** (1983) 133.
12. F. Goodridge, C.J.H. King and A.R. Wright, *Electrochim. Acta* **22** (1977) 347.
13. F. Goodridge, C.J.H. King and A.R. Wright, *Electrochim. Acta* **22** (1977) 1087.
14. R. Alkire, *J. Electrochem. Soc.* **120** (1973) 900.
15. N.P. Brandon, G.H. Kelsall and Q. Yin, Simultaneous Recovery of Lead and Lead Dioxide from Battery Effluent, Proc. Electrochem. Soc.: Energy and Electrochemical Processes for a Cleaner Environment, 2001. 2001–23 (Electrochem. Soc., N.J. 2001), pp. 306.
16. N.P. Brandon, D. Pilone, G.H. Kelsall and Q. Yin, *J. Appl. Electrochem.* **33** (2003) 853.
17. T.F. Sharpe, *in* A.J. Bard (Ed.), 'Encyclopedia of electrochemistry of the elements, vol. 1' (Marcel Dekker, New York, 1973), p. 263.

18. A.J. Appleby, H. Kita, M. Chamla, G. Bronoel, *in* A.J. Bard (Ed.), 'Encyclopedia of electrochemistry of the elements, vol. 9' (Marcel Dekker, New York, 1973), pp. 523.
19. R. Carta, S. Palmas, A.M. Polcaro and G. Tola, *J. Appl. Electrochem.* **21** (1991) 793.
20. R.W. Meredith and C.W. Tobias, *in* P. Delahay and C.W. Tobias (Eds), 'Advances in Electrochemistry and Electrochemical Engineering, vol. 2' (Wiley, New York, 1962), p. 15.
21. C. Oloman, *J. Electrochem. Soc.* **138** (1991) 2330.
22. D. Tromans, *Hydrometallurgy* **48** (1998) 327.